Articles

Spontaneous Chiral Induction in a Cubic Phase

Takashi Kajitani,[†] Shigeo Kohmoto,[‡] Makoto Yamamoto,[‡] and Keiki Kishikawa*[,‡]

Quality Materials Science, Graduate School of Science and Technology, and Department of Applied Chemistry and Biotechnology, Faculty of Engineering, Chiba University, 1-33 Yayoi-cho, Inage-ku, Chiba 263-8522, Japan

Received December 27, 2004. Revised Manuscript Received May 24, 2005

The optical property and the molecular packing structure of achiral bent-rod-shaped liquid crystalline compound **1** possessing an amide group and a flexible spacer were investigated by polarized optical microscopy (POM), circular dichroism (CD) spectroscopy, and X-ray diffraction (XRD). The molecules generated highly ordered liquid crystal phases by lateral intermolecular hydrogen bonds. The cubic phase observed in this study showed a chirality in CD spectroscopy even without the aid of a dopant. Further, its chirality was enhanced by doping with chiral dopant compound **4**. The origin of the spontaneous chiral induction was postulated, and the packing structure in the aggregates was proposed.

Introduction

Spontaneous chiral induction in the fluid phase is more difficult than that in the crystal phase. It is known that only one type of achiral molecule (a banana-shaped molecule) generated chiral layer structures in smectic liquid crystal phases.[1,2] Spontaneous chiral induction has not been reported in the other liquid crystal phases such as nematic, columnar, and cubic phases. We believe that cubic phases are the most potent phase for realizing spontaneous chiral induction, because the phases have three-dimensional superstructures in which the molecular movement is highly restricted like that in the crystal phase.[3−5] In general, hydrogen bonding is the main attractive intermolecular force in cubic phases.[4] Accordingly, it was assumed that increasing the strength of the hydrogen bonds was a key for realization of a spontaneous chiral induction in a cubic phase without the aid of a chiral dopant.

In this study, we synthesized **1a** and **1b**, which were expected to generate strong intermolecular hydrogen bonds in liquid crystal phases, and investigated their phase transitions, layer structures, optical properties, and the strengths of their intermolecular hydrogen bonds. As a result, we found the first example that achiral molecules generated a chiral cubic liquid crystal phase.

In our previous papers, we reported a methodology to increase the strength of lateral hydrogen bonds between rodlike liquid crystalline molecules by introduction of both "anchoring" and "spinning" parts in a molecule (Scheme 1a).[6] The alkoxy group laterally introduced worked as a brake in the molecular spinning to stabilize the intermolecular hydrogen bonding, and the straight-rod-shaped mesogenic unit worked as a spinning part rotating independently to stabilize the liquid crystal phase. However, the strength of the hydrogen bond was not enough to organize the molecules

* To whom correspondence should be addressed. E-mail: kishikawa@faculty.chiba-u.jp.

[†] Quality Materials Science, Graduate School of Science and Technology.

[‡] Department of Applied Chemistry and Biotechnology, Faculty of Engineering.

(1) Niori, T.; Sekine, T.; Watanabe, J.; Furukawa, T.; Takezoe, H. *J. Mater. Chem.* **1996**, *6*, 1231.

(2) (a) Niori, T.; Sekine, T.; Watanabe, J.; Furukawa, T.; Takezoe, H. *Mol. Cryst. Liq. Cryst.* **1997**, *301*, 337. (b) Sekine, T.; Takahashi, Y.; Niori, T.; Watanabe, J.; Takezoe, H. *Jpn. J. Appl. Phys.* **1997**, *36*, L69. (c) Weissflog, W.; Nádasi, H.; Dunemann, U.; Pelzl, G.; Diele, S.; Eremin, A.; Kresse, H. *J. Mater. Chem.* **2001**, *11*, 2748. (d) Pelzl, G.; Diele, S.; Weissflog, W. *Adv. Mater.* **1999**, *11*, 707. (e) Rouillon, J. C.; Marcerou, J. P.; Laguerre, M.; Nguyen, H. T.; Achard, M. F. *J. Mater. Chem.* **2001**, *11*, 2946. (f) Weissflog, W.; Wirth, I.; Diele, S.; Pelzl, G.; Schmalfuss, H.; Schoss, T.; Würflinger, A. *Liq. Cryst.* **2001**, *28*, 1603. (g) Bedel, J. P.; Rouillon, J. C.; Marcerou, J. P.; Laguerre, M.; Nguyen, H. T.; Achard, M. F. *Liq. Cryst.* **2001**, *28*, 1285. (h) Jákli, A.; Krüerke, D.; Sawade, H.; Heppke, G. *Phys. Rev. Lett.* **2001**, *86*, 5715. (i) Nakata, M.; Link, D. R.; Araoka, F.; Thisayukta, J.; Takanishi, Y.; Ishikawa, K.; Watanabe, J.; Takezoe, H. *Liq. Cryst.* **2001**, *28*, 1301. (j) Imase, T.; Kawauchi, S.; Watanabe, J. *J. Mol. Struct.* **2001**, *560*, 275. (k) Wirth, I.; Diele, S.; Elemin, A.; Pelzl, G.; Grande, S.; Kovalenko, L.; Pancenko, N.; Weissflog, W. *J. Mater. Chem.* **2001**, *11*, 1642. (l) Dantlgraber, G.; Baumeister, U.; Diele, S.; Kresse, H.; Lühmann, B.; Lang, H.; Tschierske, C. *J. Am. Chem. Soc.* **2002**, *124*, 14852. (m) Pelzl, G.; Eremin, A.; Diele, S.; Kresse, H.; Weissflog, W. *J. Mater. Chem.* **2002**, *12*, 2591. (n) Csorba, K. F.; Vajda, A.; Galli, G.; Jákli, A.; Demus, D.; Holly, S.; Baitz, E. G. *Macromol. Chem. Phys.* **2002**, *203*, 1556. (o) Takanishi, Y.; Izumi, T.; Watanabe, J.; Ishikawa, K.; Takezoe, H.; Iida, A. *J. Mater. Chem.* **1999**, *9*, 2771. (p) Yoshizawa, A.; Yamaguchi, A. *Chem. Commun.* **2002**, 2060. (q) Weissflog, W.; Ritchter, S.; Dietzmann, E.; Risse, J.; Diele, S.; Schiller, P.; Pelzl, G. *Cryst. Res. Technol.* **1997**, *32*, 271. (r) Nishiyama, I.; Yamamoto, J.; Goodby, J. W.; Yokoyama, H. *J. Mater. Chem.* **2002**, *12*, 1709. (s) Shen, D.; Diele, S.; Wirth, I.; Tschierske, C. *Chem. Commun.* **1998**, 2573. (t) Shen, D.; Diele, S.; Pelzl, G.; Wirth, I.; Tschierske, C. *J. Mater. Chem.* **1999**, *9*, 661. (u) Shen, D.; Pegenau, A.; Diele, S.; Wirth, I.; Tschierske, C. *J. Am. Chem. Soc.* **2000**, *122*, 1593. (v) Kishikawa, K.; Muramatsu, N.; Kohmoto, S.; Yamaguchi, K.; Yamamoto, M. *Chem. Mater.* **2003**, *15*, 3443. (w) Nozary, H.; Piguet, C.; Rivera, J.-P.; Tissot, P.; Morgantini, P.-Y.; Weber, J.; Bernardinelli, G.; Bünzli, J.-C. G.; Deschenaux, R.; Donnio, B.; Guillon, D. *Chem. Mater.* **2002**, *14*, 1075.

10.1021/cm0477319 CCC: $30.25
Published on Web 06/29/2005

Scheme 1. Schematic Design of the Bent-Rod-Shaped Molecules with a Spinning and Anchoring Part (a) and Also with a Spacer between Both Parts (b)

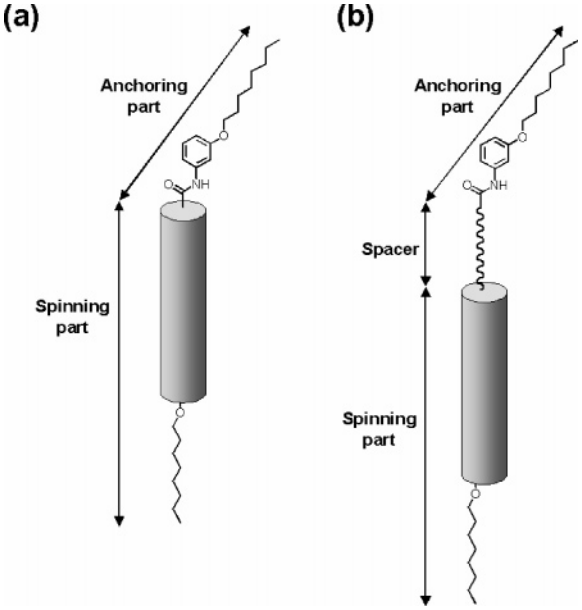

into a laterally linear molecular aggregate, because the spinning of the anchoring part could not be suppressed sufficiently. To suppress the spinning, introduction of a flexible spacer between the spinning and anchoring parts was proposed in this study (Scheme 1b). We expected that the lateral intermolecular hydrogen bonds became stronger by separating the spinning part from the anchoring part.

Results and Discussion

Synthesis. The synthetic pathways of compounds **1** are shown in Scheme 2. Compounds **1a** and **1b** (n = 5 and 10, respectively) were synthesized by the Sonogashira−Hagihara coupling reaction[7] of iodophenol derivatives **3a** and **3b** prepared by amidation of *m*-octyloxyaniline (**2**).[6]

Thermodynamic Behavior of Compounds 1 and Identification of the Phases. The behaviors of liquid crystalline

Scheme 2. Synthesis of 1

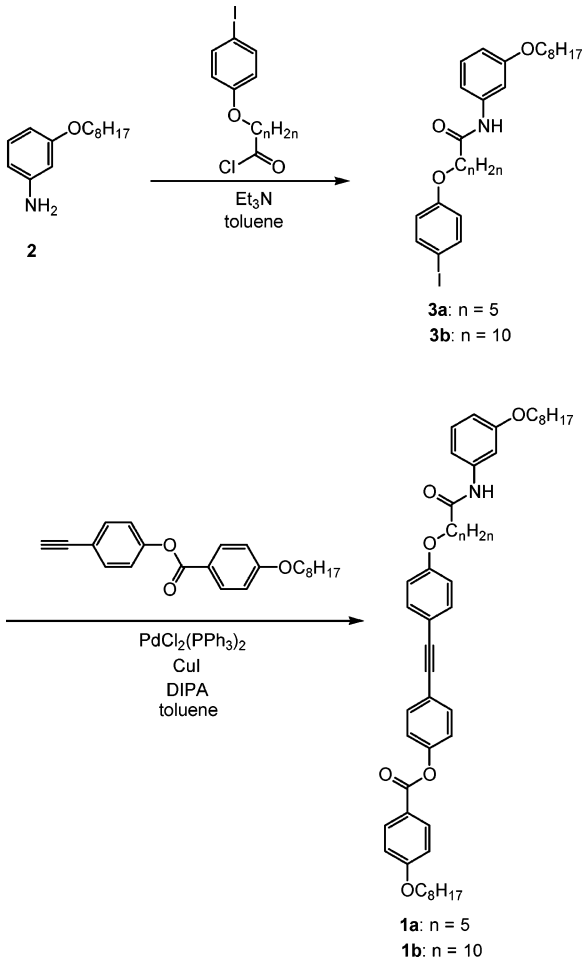

Table 1. Phase Behaviors of Compounds 1

compound	n	behavior[a]
1a	5	Cr 114(8.0) SmC 132(0.70) / 131(-0.66) N 145(0.20) / 144(-0.20) Iso; Cr 84(-4.5) SmX 91(-0.16) SmC
1b	10	Cr 106(8.8) SmC 112(0.07) / 111(-0.10) N 131(0.20) / 130(-0.20) Iso; Cr 106(9.7) Cubic[b] 97(-9.5) SmC

[a] The transition temperatures (°C) and enthalpies (in parentheses, kcal/mol) were determined by DSC (5 °C/min) and are given above and below the arrows. Cr, SmX, SmC, N, and Iso indicate crystal, smectic X, smectic C, nematic, and isotropic phases, respectively. [b] The crystallization process was too slow to be measured by DSC (about one week at room temperature).

compounds **1** are shown in Table 1. The phase identification was performed by POM. Compound **1a** (n = 5) showed enantiotropic nematic and smectic C phases, and a monotropic smectic X phase. As shown in the DSC thermogram (Figure 1), two phase transition peaks corresponding to SmC−SmX and SmX−Cr were observed. In the smectic C

(3) (a) Takanishi, Y.; Ogasawara, T.; Yoshizawa, A.; Umezawa, J.; Kusumoto, T.; Hiyama, T.; Ishikawa, K.; Takezoe, H.; Ema, K. *J. Mater. Chem.* **2002**, *12*, 1325. (b) Takanishi, Y.; Yoshida, S.; Ogasawara, T.; Ishikawa, K.; Takezoe, H. *Mol. Cryst. Liq. Cryst.* **2003**, *401*, 133. (c) Takanishi, Y.; Takezoe, H.; Yoshizawa, A.; Kusumoto, T.; Hiyama, T. *Mol. Cryst. Liq. Cryst.* **2000**, *347*, 257. (d) Yoshizawa, A.; Ise, N.; Kusumoto, T.; Takanishi, Y.; Takezoe, H.; Hiyama, T. *Mol. Cryst. Liq. Cryst.* **2001**, *364*, 271.

(4) (a) Diele, S.; Göring, P. Thermotropic Cubic Phases. *Handbook of Liquid Crystals*; Wiley-VCH: New York, 1998; Vol. 2B, Chapter XIII. (b) Lee, M.; Cho, B.-K.; Jang, Y.-G.; Zin, W.-C. *J. Am. Chem. Soc.* **2000**, *122*, 7449. (c) Li, Y.; Lin, S.-T.; Goddard, W. A., III. *J. Am. Chem. Soc.* **2004**, *126*, 1872. (d) Cheng, X.; Das, M. K.; Diele, S.; Tschierske, C. *Langmuir* **2002**, *18*, 6521. (e) Ivanova, R.; Lindman, B.; Alexandridis, P. *Langmuir* **2000**, *16*, 9058. (f) Rodriguez, C.; Kunieda, H. *Langmuir* **2000**, *16*, 8263. (g) Kato, T.; Matsuoka, T.; Nishii, M.; Kamikawa, Y.; Kanie, K.; Nishimura, T.; Yashima, E.; Ujiie, S. *Angew. Chem., Int. Ed.* **2004**, *43*, 1969. (h) Bruce, D. W. *Acc. Chem. Res.* **2000**, *33*, 831. (i) Ryu, J.-H.; Oh, N.-K.; Zin, W.-C.; Lee, M. *J. Am. Chem. Soc.* **2004**, *126*, 3551. (j) Cho, B.-K.; Lee, M. *J. Am. Chem. Soc.* **2001**, *123*, 9677. (k) Lee, M.; Cho, B.-K.; Kim, H.; Yoon, J.-Y.; Zin, W.-C. *J. Am. Chem. Soc.* **1998**, *120*, 9168. (l) Dukeson, D. R.; Ungar, G.; Balagurusamy, V. S. K.; Percec, V.; Johansson, G. A.; Glodde, M. *J. Am. Chem. Soc.* **2003**, *125*, 15974. (m) Yeardley, D. J. P.; Ungar, G.; Percec, V.; Holerca, M. N.; Johansson, G. *J. Am. Chem. Soc.* **2000**, *122*, 1684.

(5) Kunieda, H.; Uddin, M. H.; Horii, M.; Furukawa, H.; Harashima, A. *J. Phys. Chem. B* **2001**, *105*, 5419.

(6) (a) Kajitani, T.; Kohmoto, S.; Yamamoto, M.; Kishikawa, K. *Chem. Mater.* **2004**, *16*, 2329. (b) Kajitani, T.; Kohmoto, S.; Yamamoto, M.; Kishikawa, K. *J. Mater. Chem.* **2004**, *14*, 3449. (c) Kajitani, T.; Kohmoto, S.; Yamamoto, M.; Kishikawa, K. *Mol. Cryst. Liq. Cryst.*, in press.

(7) Sonogashira, K.; Tohda, Y.; Hagihara, N. *Tetrahedron Lett.* **1975**, *50*, 4467.

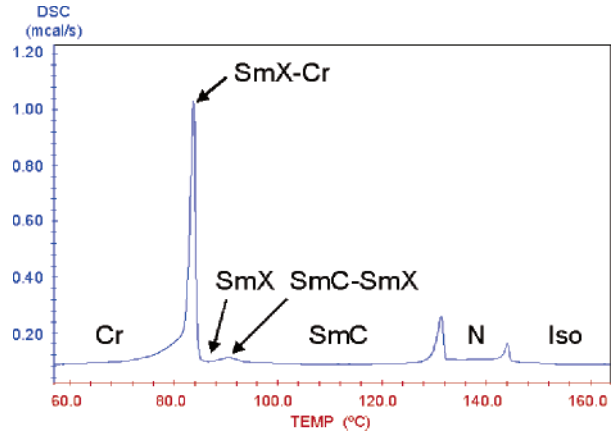

Figure 1. DSC chart of **1a**.

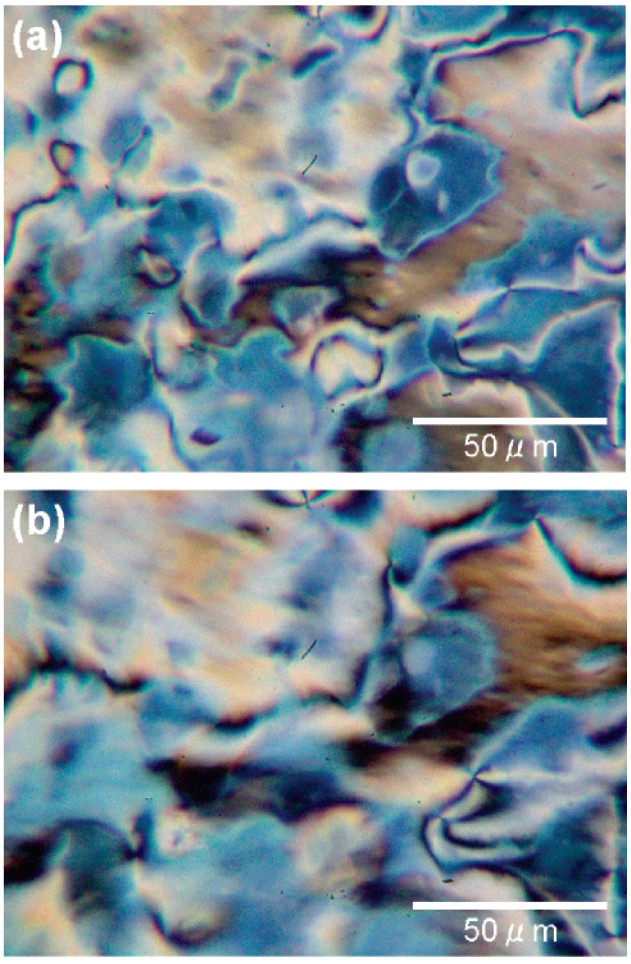

Figure 2. Polarized optical microphotographs of **1a** on cooling (600×): (a) smectic C phase at 100 °C; (b) smectic X phase at 88 °C.

phase, lines of the schlieren texture were observed clearly in POM (Figure 2a).[8] However, the lines became dim during the SmC−SmX transition on cooling (Figure 2b). From the results, it was assumed that the layer structure in the smectic X phase was more ordered than that in the smectic C phase.

Compound **1b** possessing a long flexible spacer ($n = 10$) showed enantiotropic nematic and smectic C phases with a monotropic cubic phase. In POM, the change of the textures

(8) (a) Nehring, J.; Saupe, A. *J. Chem. Soc., Faraday Trans. 2* **1972**, *68*, 1. (b) Sackmann, H.; Demus, D. *Fortschr. Chem. Forsch.* **1969**, *12*, 349. (c) Saupe, A. *Mol. Cryst. Liq. Cryst.* **1969**, *7*, 59.

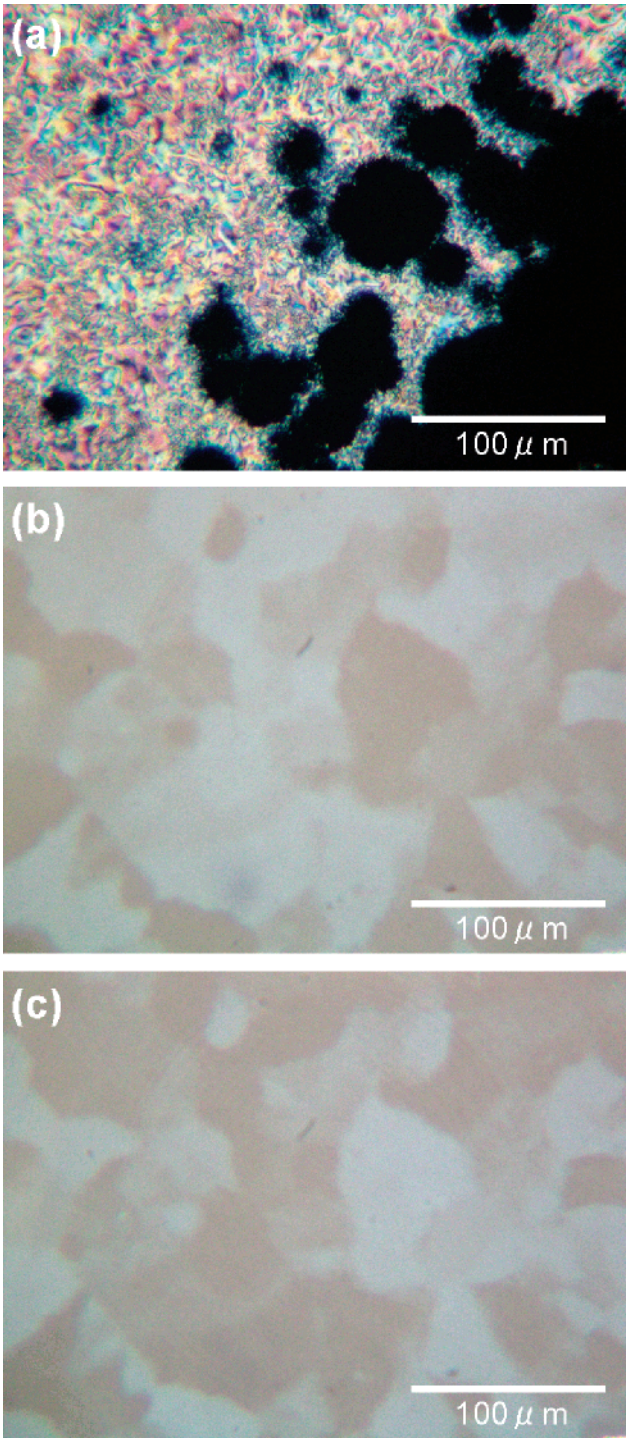

Figure 3. Polarized optical microphotographs of **1b** on cooling (300×): (a) smectic C (left) and cubic (right) phases at 97 °C; (b, c) cubic phase at 90 °C which was obtained by (b) a clockwise rotation (+5°) of the analyzer from the cross-polarization position and (c) a counterclockwise rotation (−5°) of the analyzer from the cross-polarization position.

at the SmC−cubic phase transition on cooling (Figure 3a) was observed dramatically. During the transition, small dark circular areas of the cubic phase came out and grew quickly in the bright schlieren texture of the smectic C phase. The enthalpy in the phase transition was as large as that in a liquid crystal to crystal phase transition (Figure 4). This indicated that the molecular arrangement in the cubic phase was significantly different from that in the smectic C phase.

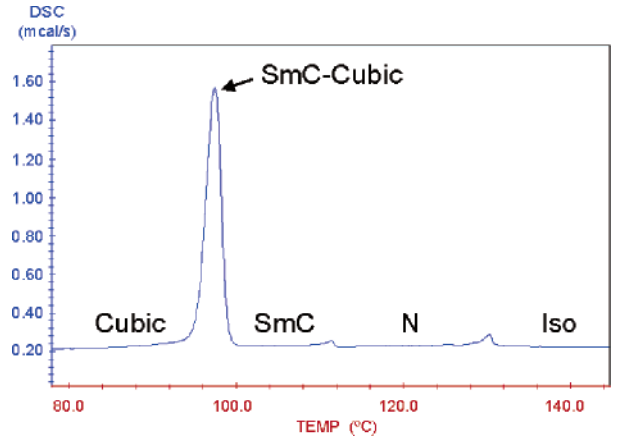

Figure 4. DSC chart of **1b**.

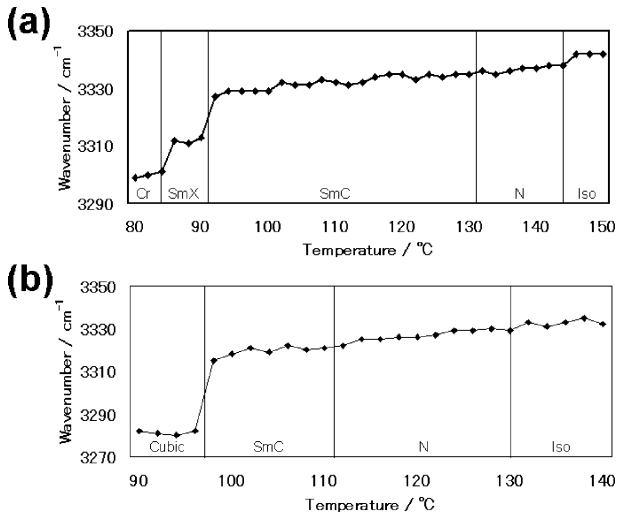

Figure 5. N−H stretching vibrations in variable-temperature FT-IR spectra on cooling: (a) **1a**; (b) **1b**.

In the cubic phase of **1b**, a mosaic plane texture was observed as the separation of bright and dark areas by a clockwise rotation (+5°) of the analyzer from the cross-polarization position (Figure 3b), because transmittance of light from one area increased and the other decreased. Then, in the case of a counterclockwise rotation (−5°) of the analyzer from the cross-polarization position (Figure 3c), the aforementioned contrast of different domains switched. This suggested that each domain was chiral and the domains had the opposite chiralities. In cubic phases, this phenomenon has not been reported yet.

Variable-Temperature FT-IR Spectra. The variable-temperature FT-IR spectra of **1a** and **1b** were measured. The wavenumbers of N−H stretching vibrations (ν_{NH}) of the amides are shown in Figure 5. It is known that the ν_{NH} decreases during the transition from an isotropic liquid to a crystal.[9] In the case of the bent-rod-shaped amides reported in our previous papers, the ν_{NH} in the smectic C phase was smaller than that in the isotropic liquid phase.[6] The shift indicated that the intermolecular hydrogen bond in the smectic C phase was stronger than that in the isotropic liquid phase. In the mesophases of compounds **1**, it was also assumed that the lateral intermolecular hydrogen bonding between the amide groups organized the molecules into a linear superstructure in the layer.

(9) Silverstein, R. M.; Bassler, G. C.; Morrill, T. C. *Spectrometric Identification of Organic Compounds*, 5th ed.; 1991.

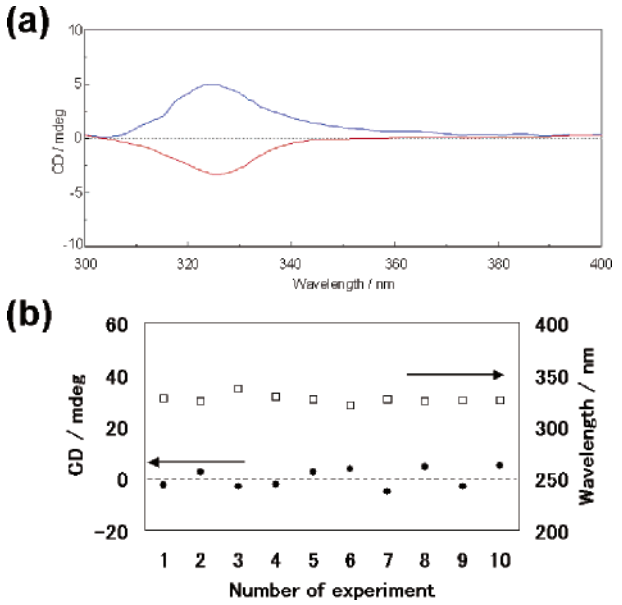

Figure 6. CD spectra of **1b** in the cubic phase: (a) the blue and red lines indicate right- and left-handed helical structures in the cubic phase, respectively; (b) the open squares and the filled circles represent the peak wavelengths and their intensities obtained by 10 runs, respectively.

The ν_{NH} of **1a** (Figure 5a) was 3342 cm^{-1} in the isotropic liquid phase. This wavenumber slightly decreased during the Iso−N transition on cooling. The value decreased gradually in the temperature range of the nematic and smectic C phases on cooling, while, during the smectic C to smectic X transition, the value decreased significantly down to approximately 3310 cm^{-1}. Thus, it was strongly assumed that the molecules in the smectic X phase were organized into linear molecular aggregates in each layer by the strong lateral intermolecular hydrogen bonds.

The ν_{NH} of **1b** in the nematic phase (Figure 5b) was slightly smaller than that in the isotropic liquid phase. The wavenumber gradually decreased in the range of the nematic and smectic C phases on cooling. Accordingly, it seemed that the molecules were arranged partially in a linear manner by the weak lateral intermolecular hydrogen bonds in the nematic and smectic C phases.[6] Then, the wavenumber decreased down to 3290 cm^{-1} during the smectic C to cubic phase transition. Thus, it was assumed that the molecules in the cubic phase were aligned rigidly and their movements were restricted by the strong intermolecular hydrogen bonds between the amide groups.

CD Spectra of Achiral Molecules of 1b in the Cubic Phase. To confirm the chirality of the domains in the cubic phase generated by the achiral molecules, the circular dichroic (CD) spectra of **1b** were measured. Each measurement was carried out, after the sample was heated to the isotropic phase and cooled to the cubic phase.[10] In Figure 6a, one positive or negative peak appeared randomly around 325 nm in each run. After 10 runs, the average of the intensity became almost zero, and the wavelengths of the peak maximum were almost constant (Figure 6b). This indicated that a right- or left-handed helical structure (or

Table 2. Phase Behavior of the Mixture of 1b and 4

mixture	weight fraction (wt%)	behavior[a]
1b + 4	95 : 5	Solid $\xrightarrow{104}$ SmC $\underset{107}{\overset{110}{\rightleftharpoons}}$ N $\underset{125}{\overset{128}{\rightleftharpoons}}$ Iso; Solid $\xrightarrow{b}$ Cubic $\underset{97}{\overset{104}{\rightleftharpoons}}$ SmC

[a] The transition temperatures (°C) were determined by POM and are given above and below the arrows. Solid, SmC, N, and Iso indicate solid, smectic C, nematic, and isotropic phases, respectively. [b] The crystallization process was too slow to be measured by DSC (about one week at room temperature).

conformation) was generated randomly in the cubic phase. In the CD experiment the beam size is about 1 mm in diameter, while the size of each domain is 10−50 μm in POM. The ratio of the opposite chiral conformers in the area measured is almost 50:50, and the number of conformers with one chirality is slightly larger than that with the other chirality. Accordingly, a very small peak was randomly obtained in the experiment (Figure 6b).

Enhancement of the Chirality in 1b by Doping with Chiral Dopant 4. To investigate the separation of domains with the opposite chiralities in the cubic phase, a small amount (5%) of chiral amide **4** was mixed with **1b**.

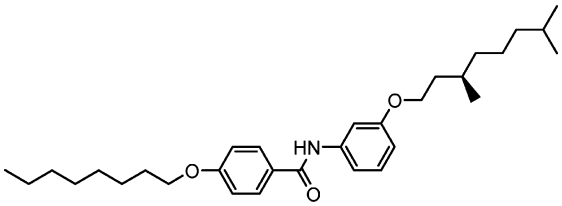

4

The phase transition behavior of the mixture is shown in Table 2. Each transition temperature of the mixture was similar to that of pure **1b**; however, their optical textures were apparently different. Comparing parts b and c of Figure 3, the domains with one chirality were observed much more than those with the other one. In clockwise and counterclockwise rotations of the analyzer from the cross-polarization position in POM, the contrast between the domains was not observed. The drastic change from pure **1b** to doped **1b** was also observed in CD. In Figure 7, only a positive peak was observed in every run at a constant wavelength of about 325 nm. This suggested that domains with one chirality were generated predominantly by doping with chiral dopant **4**.

X-ray Diffraction of 1. To identify the superstructures of **1** in the liquid crystal phases, powder X-ray diffraction (XRD) was carried out. The peaks of *d*(100), *d*(111), *d*(200), and *d*(220) are shown in Table 3. The *d*(100) value of **1a** in the smectic X phase (30.7 Å) was shorter than that in the smectic C phase (37.1 Å). The molecular tilt angle in the smectic X phase (52°) was larger than that in the smectic C phase (42°).

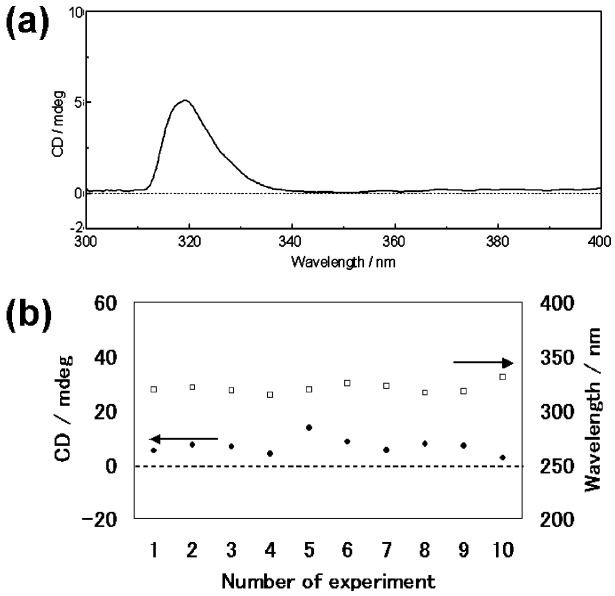

Figure 7. CD spectra of **1b** doped with 5% **4** in the cubic phase: (a) one of the CD spectra; (b) the open squares and the filled circles show the peak wavelengths and their intensities by 10 runs, respectively.

The XRD patterns of **1b** in the cubic phase are shown in Figure 8a. Five peaks were observed. The reciprocal spacing of those peaks was found to be in the ratio of $1:\sqrt{3}:\sqrt{4}:\sqrt{8}:\sqrt{11}$. We considered that the five peaks represent diffractions from the (100), (111), (200), (220), and (311) planes, respectively. If the chirality is not considered, the ratio of the reflections suggests an *Fm*3*m* phase, though a *Pn*3*m* lattice is possible if one assumes that an additional reflection corresponding to $\sqrt{2}$ (a diffraction from the (110) plane) is very weak. We repeated the XRD measurement many times, but we could not observe the (110) peak of *Pn*3*m*. So, from our results, we think that *F*432 is the most suitable for the chiral fcc lattice structure. The face-centered cubic (fcc) lattice structure includes the four spheroidic aggregates.[5] The *z* value was calculated on the basis of the cell lattice (a = 60 Å) to give z = 80. This means that about 80 molecules are in the lattice and each spheroidic aggregate is composed of approximately 20 molecules. The growth of a broad peak around 20° was observed after the sample was allowed to stand at room temperature for a week (Figure 8b,c). This means that the cubic phase in a supercooled state crystallizes gradually at room temperature.

On the other hand, the tilt angle (31°) in the smectic C phase of **1b** was nearly in accordance with that of the smectic C phase (about 30°) reported in our previous paper in which weak lateral intermolecular hydrogen bonds were observed.[6]

Models for the Molecular Aggregates of 1 in Liquid Crystal Phases. On the basis of these analytical results, we postulated models for the molecular aggregates in the mesophases of **1**. As shown in Figure 9a, it can be assumed that compound **1a** possessing a short flexible spacer (n = 5) generates the partially syn-parallel self-assemblies in the smectic C phase by weak hydrogen bonding, which was estimated from the variable-temperature FT-IR spectra, while, in the smectic X phase, the molecules bound with the strong intermolecular hydrogen bonds organize in syn-parallel linear molecular aggregates in the layer (Figure 9b). The aggregates

(10) (a) Thisayukta, J.; Nakayama, Y.; Kawauchi, S.; Takezoe, H.; Watanabe, J. *J. Am. Chem. Soc.* **2000**, *122*, 7441. (b) Thisayukta, J.; Niwano, H.; Takezoe, H.; Watanabe, J. *J. Mater. Chem.* **2001**, *11*, 2717. (c) Thisayukta, J.; Niwano, H.; Takezoe, H.; Watanabe, J. *J. Am. Chem. Soc.* **2002**, *124*, 3354.

Table 3. XRD Data of 1

compd	*n*	molecular length, Å	temp, °C	phase	*d*(100), Å	*d*(111), Å	*d*(200), Å	*d*(220), Å	*d*(100)/*l*	tilt angle, °C
1a	5	49.8	90	SmX	30.7		15.3		0.62	52
			100	SmC	37.1		18.9		0.74	42
			110		37.1		18.8		0.74	42
			120		37.1		18.8		0.74	42
			130		37.0		18.8		0.74	42
1b	10	60.4	80	cubic	46.5	25.5	22.8	16.3	0.77	
			90		46.5	25.4	22.6	16.5	0.77	
			100		47.1	25.7	23.3	16.7	0.78	
			110	SmC	51.5		25.6		0.85	31

may also form the antiparallel superstructure to cancel out their macroscopic dipoles (Figure 10) because the broad peak at 9.8 Å which corresponds to twice the thickness of the linear aggregate was observed.[11]

The smectic C phase of **1b** ($n = 10$) also gave results similar to those of **1a** in variable-temperature FT-IR spectra and XRD. It was thought that the smectic C phase also had partially syn-parallel aggregates in the layers. In variable-temperature FT-IR spectroscopy, the cubic phase of **1b** indicated the very strong intermolecular hydrogen bonds of the amides, which enabled the continuous syn-parallel arrangement like that in Figure 9b to be generated.

The molecular packing model of the chiral cubic phase was estimated on the basis of the fcc symmetry and the *z* value as follows. In an fcc lattice it is known that 12 spheroidic aggregates are arranged equivalently around each spherical aggregate. Accordingly, the rodlike cores of the spherical aggregate must be arranged equivalently in the 12 directions to show the optically isotropic property. This suggests that the most suitable number of molecules in each of the spheroidic aggregates is 24, on the basis of $z/4 = 20$ ($z = 80$, and the fcc lattice includes four spheroidic aggregates). In the spheroidic aggregate (Figure 11a), the

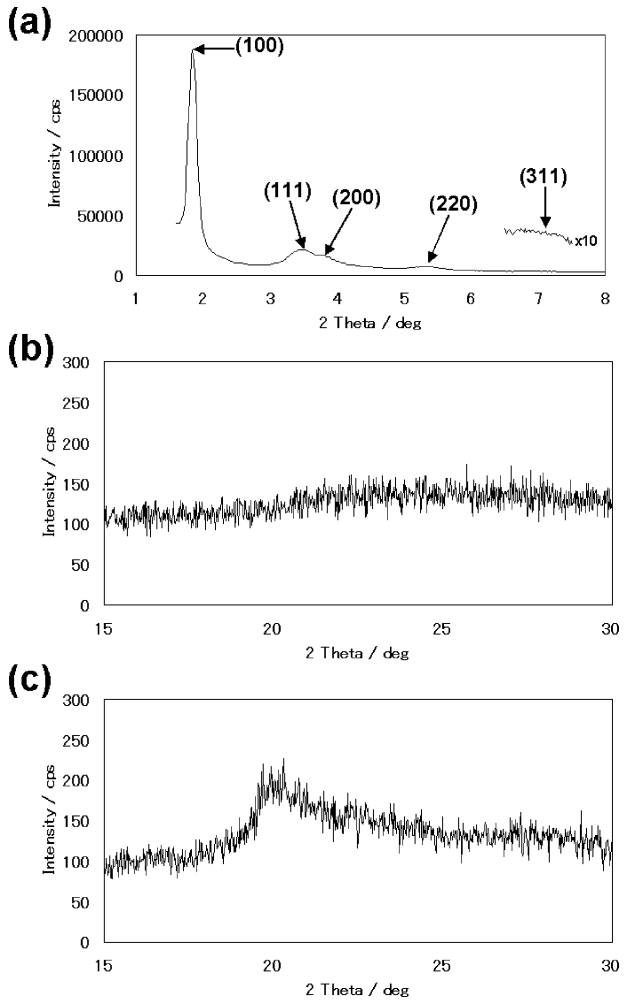

Figure 8. X-ray diffraction patterns of **1b**: (a) small-angle diffraction pattern in the cubic phase at 90 °C; (b) wide-angle halos in the supercooled cubic phase at room temperature; (c) one broad peak around 20° was observed after 7 days.

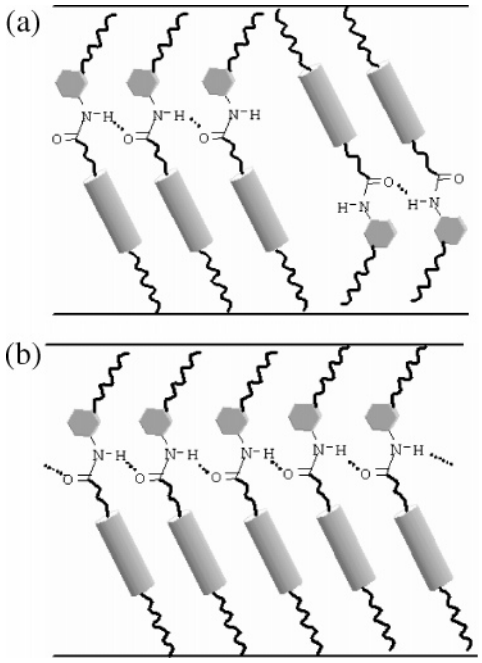

Figure 9. Molecular packings of **1**: (a) partially syn-parallel self-assemblies in the smectic C phases by weak lateral intermolecular hydrogen bonds; (b) a linear self-assembly in a syn-parallel arrangement in the smectic X and the cubic phases by continuous intermolecular hydrogen bonds. The dashed lines indicate the hydrogen bonds.

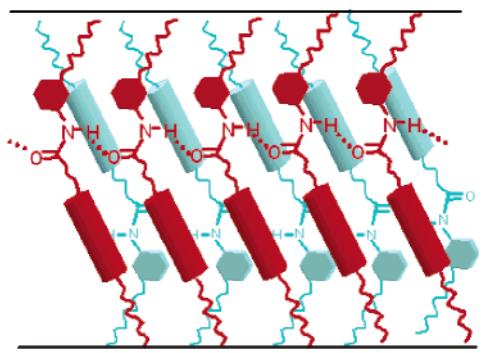

Figure 10. Schematic molecular packing structure of **1a** in the smectic X phase. The molecules are aligned by linear intermolecular hydrogen bonds, and the linear aggregates are arranged in an antiparallel manner to cancel out the macroscopic dipoles in the layer.

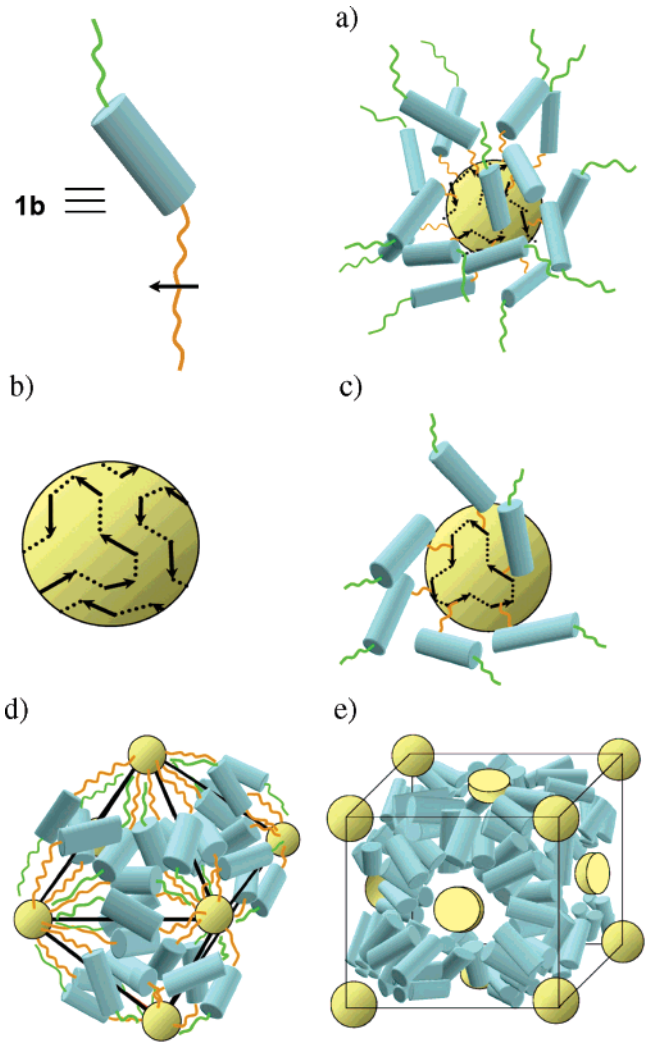

Figure 11. Schematic representation of the molecular packing structure in the cubic phase of **1b**: (a) twenty-four rods on the sphere consisting of twenty-four octyloxyphenylamides linked with hydrogen bonds, (b) hydrogen bond network of the spheroidic aggregate consisting of octyloxyphenylamides (four sets of cyclic networks on the sphere), (c) cyclic hydrogen bond network of six amides and six tilted rods (the arrows indicate the directions of the intermolecular hydrogen bonds), (d) octahedron filled with rods, alkyl chains, and spheroidic octyloxyphenylamide aggregates, and (e) fcc lattice including ninety-six rods.

24 rods are outside of the sphere consisting of the 24 octyloxyphenylamide moieties hydrogen-bonded intermolecularly. There are four sets of cyclic hydrogen bond networks of the amides on the sphere (Figure 11b). Each cyclic network consists of six octyloxyphenylamide moieties, and the six rods are outside of it (Figure 11c). In Figure 11d, the octahedron (as a part of the fcc lattice) has the spheroidic octylphenylamide aggregates at every corner. At each line, both of the terminal aggregates supply two rods to generate the C_4 symmetric tetramer. The rods and the spheroidic octyloxyphenylamide aggregates in the fcc lattice are indicated in Figure 11e. In this model, each of the alkyl chains, rodlike cores, and the amide parts segregates into its own subspace.

Origin of the Chiral Induction. The CD spectra of **1b** in the cubic phase indicated the existence of chirality in each domain. It is assumed that the CD signal at 325 nm is ascribed to a chiral molecular conformation. The steric hindrance and hydrogen bonding of the anchoring part suppress the free rotation of the anchoring part in the molecules, although the spinning part is still spinning freely. In the AM1 calculation of **1b**,[12] the angle generated by the amide carbonyl group and benzene ring was about 0° in the most stable conformer **A** (Figure 12). However, in the case of **A**, the lateral intermolecular hydrogen bonds cannot be formed strongly because of the steric repulsion between the *m*-alkoxyphenyl groups (Figure 13a). Accordingly, the molecules change their conformation to a slightly twisted one to form strong hydrogen bonds between the amide groups (Figure 13b). The twist generates chirality in the molecule. Although the twisted conformer is less stable than the plane conformer (**A**), the twisted conformation is stabilized by the strong hydrogen bonding. Hydrogen bonding between the *P*-conformers (Figure 13b) was preferable over that between the *P*- and *M*-conformers (Figure 13c). The shape-fitting of one molecule with the other molecules is significant during the packing process in the liquid crystal as well as that in the crystal.[13] In the case of **1b**, it is assumed that the conformer with the same chirality dominates in one of the unit cells.

Conclusion

In this study, we could demonstrate that the methodology, introduction of a flexible spacer between the spinning and anchoring parts, is effective to strengthen the lateral intermolecular hydrogen bonding in the mesophase. To the best of our knowledge, this is the first example of spontaneous chiral induction in a cubic phase by achiral molecules. It is assumed that our methodology can be applied to construct hydrogen bond networks in the mesophase. Further study of absolute chiral inductions in the mesophase is now in progress.

Experimental Section

The typical procedure of **1** and spectral data of **1** and **4** are shown below. The synthetic procedure of **4** was described in our preceding paper (*Chem. Mater.* **2004**, *16*, 2329.).

A Typical Procedure for Synthesis of 1. To a 100 mL Schlenk flask were added **3a** (0.27 g, 0.50 mmol), 4-ethynylphenyl 4-octyloxybenzoate (0.26 g, 0.75 mmol), *trans*-dichlorobis(triphenylphosphine)palladium(II) (18.0 mg, 2.5×10^{-2} mmol), copper(I) iodide (3.0 mg, 1.5×10^{-2} mmol), and dry toluene (30 mL). The air was replaced with argon, and diisopropylamine (0.210 mL, 1.51 mmol) was added by a syringe through a rubber septum. The

(11) (a) Eichhorn, S. H.; Paraskos, A. J.; Kishikawa, K.; Swager, T. M. *J. Am. Chem. Soc.* **2002**, *124*, 12742. (b) Matsunaga, Y.; Hikosaka, L.; Hosono, K.; Ikeda, N.; Sakatani, T.; Sekiba, K.; Takachi, K.; Takahashi, T.; Uemura, Y. *Mol. Cryst. Liq. Cryst.* **2001**, *363*, 51. (c) Yayloyan, S. M.; Bezhanova, L. S.; Abrahamyan, E. B. *Ferroelectrics* **2000**, *245*, 147. (d) Kishikawa, K.; Miwa, Y.; Kurosaki, T.; Kohmoto, S.; Yamamoto, M.; Yamaguchi, K. *Chem. Mater.* **2001**, *13*, 2468. (e) Kajitani, T.; Miwa, Y.; Igawa, N.; Katoh, M.; Kohmoto, S.; Yamamoto, M.; Yamaguchi, K.; Kishikawa, K. *J. Mater. Chem.* **2004**, *14*, 2612.

(12) AM1 calculation was carried out using the software WinMOPAC Ver.3.5 (Fujitsu, Ltd.). Stewart, J. J. P. *J. Comput. Chem.* **1989**, *10*, 209−220, 221−264.

(13) Kajitani, T.; Masu, H.; Kohmoto, S.; Yamamoto, M.; Yamaguchi, K.; Kishikawa, K. *J. Am. Chem. Soc.* **2005**, *127*, 1124.

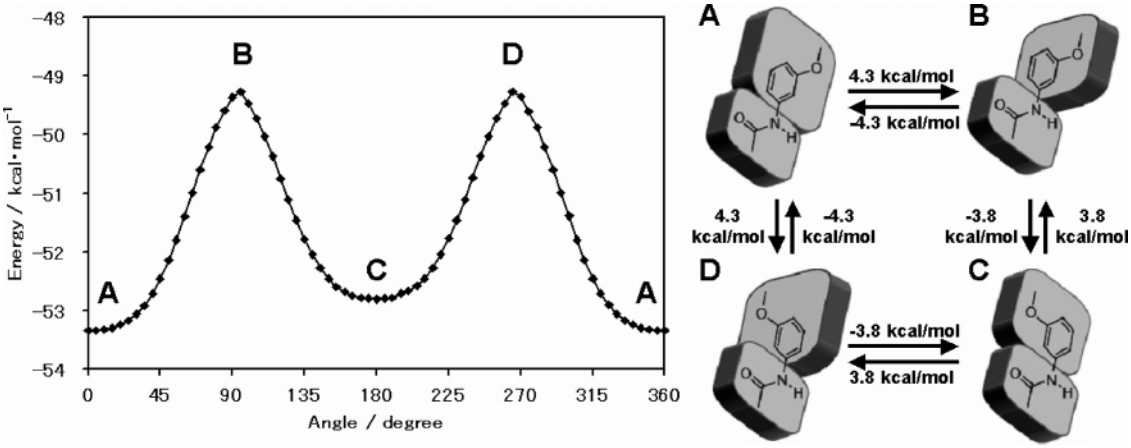

Figure 12. Proposed conformations of **1**. The planar conformers (**A** and **C**) are more stable than the twisted conformers (**B** and **D**).

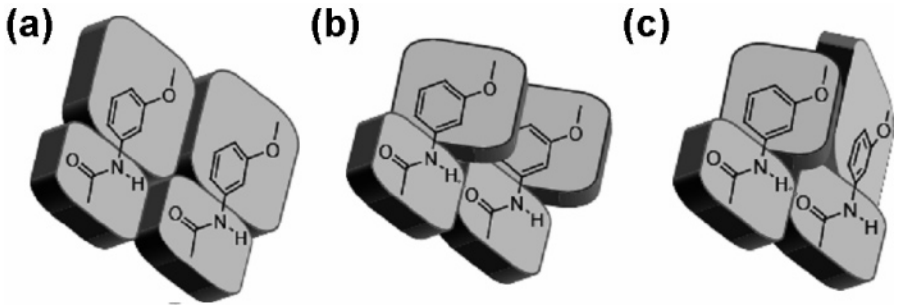

Figure 13. Molecular arrangements of the conformers in the hydrogen bonding of amide **1**: (a) side-by-side arrangement of two planar conformers **A**; (b) a pair of *P*-conformers with intermolecular hydrogen bonding; (c) *P*- and *M*-conformers with intermolecular hydrogen bonding.

mixture was stirred at reflux for 4 h. The solution was washed with 1 N HCl (50 mL), water (50 mL), and an aqueous solution of $NaHCO_3$ (50 mL) and dried over $MgSO_4$. The crude product was purified by silica gel chromatography (25% chloroform−hexane) to give **1a** as a pale yellow solid (0.12 g, 45.8%).

Data for 1a: yield 45.8%; pale yellow solid (methanol−ethyl acetate); IR (KBr) 3298, 2922, 2854, 1725, 1657, 1606, 1514, 1468, 1249, 1168, 761, 684 cm^{-1}; ^1H NMR (500 MHz, $CDCl_3$) δ 0.88 (t, 3H, $J = 7.0$ Hz), 0.90 (t, 3H, $J = 7.0$ Hz), 1.28−1.35 (m, 20H), 1.40−1.50 (t, 4H, $J = 7.5$ Hz), 1.76 (t, 2H, $J = 7.5$ Hz), 1.82 (t, 4H, $J = 7.5$ Hz), 2.38 (t, 2H, $J = 7.5$ Hz), 3.94 (t, 2H, $J = 6.6$ Hz), 3.98 (t, 2H, $J = 7.0$ Hz), 4.04 (t, 2H, $J = 6.6$ Hz), 6.65 (d, 1H, $J = 6.5$ Hz), 6.85 (d, 2H, $J = 8.8$ Hz), 6.92 (d, 1H, $J = 7.9$ Hz), 6.97 (d, 2H, $J = 8.9$ Hz), 7.12 (s, 1H), 7.17 (t, 1H, $J = 6.7$ Hz), 7.19 (d, 2H, $J = 8.6$ Hz), 7.31 (s, 1H), 7.45 (d, 2H, $J = 8.9$ Hz), 7.55 (d, 2H, $J = 8.9$ Hz), 8.13 (d, 2H, $J = 8.9$ Hz); ^{13}C NMR (125.65 MHz, $CDCl_3$) δ 14.30, 22.87, 25.42, 25.95, 26.20, 26.25, 29.18, 29.31, 29.43, 29.45, 29.47, 29.53, 29.57, 32.01, 32.03, 37.88, 67.93, 68.29, 68.58, 87.60, 89.66, 106.25, 110.97, 111.75, 114.57, 114.77, 115.39, 121.38, 121.55, 122.10, 129.81, 132.54, 132.78, 133.27, 150.91, 159.35, 160.03, 163.88, 164.92. Anal. Calcd for $C_{49}H_{61}NO_6$: C, 77.44; H, 8.09; N, 1.84. Found: C, 77.19; H, 7.96; N, 1.78.

Data for 1b: yield 38.6%; white solid (methanol−ethyl acetate); IR (KBr) 3287, 3066, 2925, 2856, 1729, 1664, 1605, 1542, 1509, 1468, 1419, 1253, 1204, 1166, 1075, 1021, 839, 767 cm^{-1}; ^1H NMR (500 MHz, $CDCl_3$) δ 0.88 (t, 6H, $J = 6.7$ Hz), 1.28−1.38 (m, 24H), 1.44 (t, 8H, $J = 7.1$ Hz), 1.67−1.84 (m, 8H), 2.31 (t, 2H, $J = 7.5$ Hz), 3.92 (t, 2H, $J = 6.6$ Hz), 3.95 (t, 2H, $J = 6.7$ Hz), 4.03 (t, 2H, $J = 6.6$ Hz), 6.63 (d, 1H, $J = 8.3$ Hz), 6.85 (d, 2H, $J = 8.6$ Hz), 6.92 (d, 1H, $J = 7.9$ Hz), 6.96 (d, 2H, $J = 8.9$ Hz), 7.16 (t, 1H, $J = 8.3$ Hz), 7.18 (d, 2H, $J = 8.3$ Hz), 7.30 (s, 1H), 7.32 (s, 1H), 7.44 (d, 2H, $J = 8.6$ Hz), 7.54 (d, 2H, $J = 8.3$ Hz), 8.12 (d, 2H, $J = 8.6$ Hz); ^{13}C NMR (100.40 MHz, $CDCl_3$) δ 14.12, 22.67, 25.55, 25.99, 26.03, 29.09, 29.18, 29.22, 29.25, 29.33, 29.37, 29.39, 29.49, 31.81, 31.82, 37.81, 68.00, 68.04, 68.34, 87.31, 89.54, 105.92, 110.60, 111.53, 114.33, 114.53, 114.96, 121.17, 121.25, 121.88, 129.52, 132.31, 132.55, 133.02, 139.22, 150.62, 159.24, 159.73, 163.65, 164.73, 171.47. Anal. Calcd for $C_{54}H_{71}NO_6$: C, 78.13, H, 8.62, N, 1.69, Found: C, 77.92, H, 8.50, N, 1.64.

Data for 4: yield 72.5%; white solid (methanol−ethyl acetate); IR (KBr) 3310, 2929, 2857, 1644, 1606, 1529, 1508, 1436, 1254, 1188, 840, 781 cm^{-1}; ^1H NMR (500 MHz, $CDCl_3$) δ 0.87 (d, 6H, $J = 6.7$ Hz), 0.89 (t, 3H, $J = 6.8$ Hz), 0.93 (d, 3H, $J = 6.8$ Hz), 1.16 (t, 4H, $J = 6.8$ Hz), 1.24−1.36 (m, 10H), 1.47 (t, 2H, $J = 7.2$ Hz), 1.53 (t, 1H, $J = 6.8$ Hz), 1.58 (t, 1H, $J = 6.8$ Hz), 1.65−1.71 (m, 2H), 1.80 (t, 2H, $J = 7.0$ Hz), 4.00 (t, 4H, $J = 6.8$ Hz), 6.68 (d, 1H, $J = 10.7$ Hz), 6.95 (d, 2H, $J = 8.6$ Hz), 7.05 (d, 1H, $J = 8.0$ Hz), 7.22 (t, 1H, $J = 5.0$ Hz), 7.42 (s, 1H), 7.79 (s, 1H), 7.81 (d, 2H, $J = 8.8$ Hz); ^{13}C NMR (125.65 MHz, $CDCl_3$) δ 14.10, 19.65, 22.62, 22.66, 22.72, 24.68, 26.00, 27.99, 29.13, 29.23, 29.34, 29.85, 31.81, 36.24, 37.32, 39.26, 66.40, 68.28, 106.26, 110.92, 111.97, 114.47, 126.88, 128.83, 129.65, 139.35, 159.84, 162.14, 165.26; $[\alpha]^{20}_D$ −5.5° ($c = 0.06$, $CHCl_3$). Anal. Calcd for $C_{31}H_{47}NO_3$: C, 77.29; H, 9.83; N, 2.91. Found: C, 77.00; H, 9.79; N, 2.66. $[\alpha]^{20}_D$ −5.5° ($c = 0.06$, $CHCl_3$).

CD Measurement of Pure 1b. Compound **1b** was sandwiched with two quartz plates (size of the quartz plate, 25 mm × 50 mm (thickness 1 mm); sample area size, 15 mm × 15 mm; sample thickness, about 4 μm). The quartz plates were heated, and the sample became an isotropic liquid. After cooling of the sample to room temperature (the temperature of the room was kept at 22 °C), the quartz plates were set in the chamber in the CD spectroscope, in which the beam direction was perpendicular to the quartz plate plane. The CD spectra were measured under a nitrogen atmosphere (beam diameter $\varphi = 1$ mm). The alignment of the sample was confirmed by polarized optical microscopy.

CM0477319